Vertical Organic Tunnel Field-Effect Transistors

Shiyi Liu,[†] Max L. Tietze,[‡,¶] Akram Al-Shadeedi,[†,§] Vikash Kaphle,[†] Changmin Keum,[†,‖] and Björn Lüssem[*,†]

†*Department of Physics, Kent State University, Kent, OH, 44240*

‡*King Abdullah University of Science and Technology, KAUST Solar Center, Physical Science and Engineering Division. Thuwal 23955-6900, Saudi Arabia*

¶ *Department of Microbial and Molecular Systems, Centre for Membrane Separations, Adsorption, Catalysis and Spectroscopy for Sustainable Solutions (cMACS), KU Leuven - University of Leuven, Celestijnenlaan 200F, B-3001, Leuven, Belgium*

§*Department of Physics, University of Baghdad, Al-Jadriya, Baghdad, 10071, Iraq*

‖*Organic Semiconductor Centre, SUPA, School of Physics & Astronomy, University of St Andrews, St Andrews, KY16 9SS, United Kingdom*

E-mail: blussem@kent.edu

Abstract

Doping organic semiconductors has become a key technology to increase the performance of organic light emitting diodes, solar cells, or field-effect transistors (OFETs). However, doping can not only be used to optimize these devices, but to enable new design principles as well. Here, a novel type of OFET is reported - the vertical organic tunnel field-effect transistor. Based on heterogeneously doped drain and source contacts, charge carriers are injected from an n-doped source electrode into the channel by Zener-tunneling and are transported toward a p-doped drain electrode. The working mechanism of these transistors is discussed with the help of a tunnel model that takes energetic broadening of transport states in organic semiconductors and roughness of organic layers into account. The proposed device principle opens new ways to optimize OFETs. It is shown that the Zener junction included between source and drain of the vertical organic tunnel field-effect transistors suppresses short channel effects and improves the saturation of vertical OFETs.

Keywords

Organic Semiconductors, Molecular Doping, vertical OFETs, p-i-n Diode, Zener Tunneling

1 Introduction

In order to compete with other technologies, organic transistors are not only required to show a high performance, i.e. high driving currents and fast switching, but to keep their advantage of being a low-cost technology. However, given the comparably low charge carrier mobilities of organic semiconductors (5-8 $cm^2V^{-1}s^{-1}$),[1] short channel lengths (i.e. below 1 μm) have to be used to reach switching frequencies above 10 MHz,[2] which usually necessitates the use of cost-intensive structuring techniques. Vertical organic transistors address this dilemma: In vertical organic transistors the channel is formed perpendicular to the substrate and the channel length can be controlled by the thickness of the organic layers down to the 10 nm range even without the use of any additional structuring method.[3]

The general setup of a vertical organic field-effect transistor (VOFET)[3–9] is sketched in Fig.1a. VOFETs consist of a gate electrode and gate dielectric on the bottom, a source electrode in the middle of the device, and a drain electrode on top. The current injected at the source electrode is modulated by the gate potential and will leave the device at the drain electrode. VOFETs were shown to surpass the performance of comparable lateral OFETs, reaching high driving currents and transconductance values.[3] Furthermore, due to their vertical structure, it is straightforward to include light emitting or absorbing layers to build light-emitting transistors or phototransistors.[10–12]

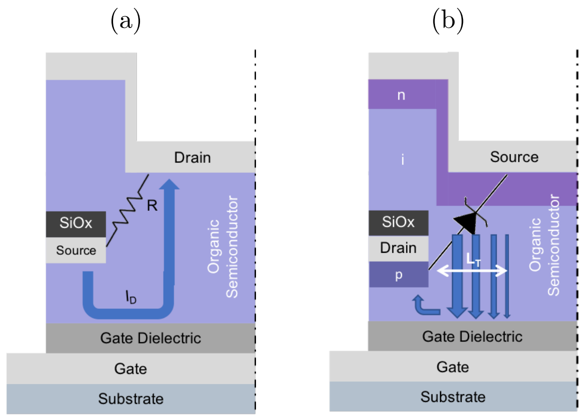

Figure 1: (a) General setup of vertical organic field-effect transistors (VOFETs). Due to the short distance between source and drain electrodes, VOFETs are prone to short channel effects. In particular, a direct leakage current between source and drain, indicated by the resistor R, leads to an insufficient saturation of the transistors. (b) Setup of a Vertical Organic Tunnel Field-Effect Transistor (VOTFET) as proposed here. In comparison to common VOFETs, the electrode in the middle of the device, operating as drain, is p-doped and electrode on the top of the transistor, operating as source, is n-doped, i.e., a p-i-n junction is formed between source and drain, suppressing direct leakage currents. To operate the VOTFET, a potential is applied between the source and gate electrode, which is sufficient to induce Zener tunneling inside the intrinsic layer. Depending on the operation regime, currents will be localized along the edge of the drain electrode. L_T indicates the characteristic localization or transfer length.

Despite these promising results, VOFETs are still facing challenges. For example, the groups of Tessler et al.[11] and Lee et al.[6] have shown that VOFETs suffer from a direct source-drain leakage that is not properly controlled by the gate electric field. This leakage path from source to drain, illustrated by a resistive element in Fig. 1a, leads to an insufficient or even absent saturation regime, which severely limits the amplification that can be obtained in this technology.

Several strategies were put forward to address this problem. It was shown that covering the source edge by an insulator reduces direct leakage from source to drain,[6,11] or that addition of an extra electrode shielding the source electrode from the drain potential can increase saturation.[11] However, these approaches rely on the use of lithographic structuring, which contradicts some of the intended low-cost advantages of VOFETs.

Here, we propose a new device architecture that can overcome these limitations - the Vertical Organic Tunnel Field-Effect Transistor (VOTFET). Inorganic Tunnel Field-Effect Transistors (TFETs), firstly reported by Hansch et al. in 2000,[13] have received considerable attention over the last decade.[14–17] Off-currents in TFETs are lower compared to standard MOSFETs, in particular for short channel lengths.[18] Furthermore, due to tunnel injection of charge carriers at the source, TFETs are not bound to the limit for the subthreshold swing of 63 mV/dec valid for FETs based on thermal injection.[18] Most recently, values such low as 15 mV/dec were demonstrated for TFETs based on vertical silicon-MoS_2 heterostructures.[19] Due to their low driving voltages, TFETs are thus promising devices for electronic applications requiring lower energy consumption.

Apart from a few reports of tunnel injection in carbon-nanotube based FETs,[17,20] TFETs based on small-molecule organic semiconductors have not been reported yet. However, several reports indicate that charge carrier tunneling is prevalent in organic semiconductors as well, e.g. in organic Zener diodes.[21,22] Zener tunneling was used to inject minority charge carriers (holes) from the source/drain contacts of an Organic Field-Effect Transistor (OFET) into its n-doped channel,[23] to design AC driven Organic Light-Emitting Diodes (OLEDs),[24] or to generate charges in stacked OLEDs.[25]

The design of the VOTFET proposed here is shown in Fig. 1b. In contrast to the common VOFET design (cf. Fig. 1a), n- and p-doped layers are introduced at the top electrode (operating as source in this design) and the middle electrodes (now operating as drain), respectively. Thus, a p-i-n junction is formed between source and drain, which, as it is operated in the backward direction, suppresses direct source-drain leakage currents. Still, a regular drain current can be injected by Zener tunneling inside the intrinsic semiconductor layer induced by the potential difference between the source and gate electrodes.

In the following, the working mechanism of the VOTFET is systematically studied by, first, characterizing tunneling in p-i-n based Zener diodes, and second, by varying the composition and structure of vertical OTFETs. In particular, it is shown that direct source-drain leakage currents are suppressed by the backward operated Zener junction formed between the source and drain electrode. Thereby, short channel effects are reduced and the saturation behavior in VOFETs is improved.

Despite optimization of the gate dielectric, leading to low voltage operation, the transistors do not reach subthreshold swings below 63 mV/dec as attainable by theory. To clarify the origin of this limitation, a qualitative analytic tunneling model is developed. With the help of this model, it is shown that the subthreshold swing of VOTFETs is currently limited by a broad density of states in organic semiconductors as well as a considerable film roughness of the intrinsic organic inter-layer, leading to a gradual onset of Zener tunneling inside the p-i-n junction.

2 Results and Discussion

2.1 Tunneling in Fullerene (C_{60})/ Pentacene based p-i-n Diodes

Zener tunneling in organic p-i-n diodes was reported e.g. by Kleemann et al.[21] and is used to generate charges in AC driven OLEDs[24] or stacked OLEDs.[26] The energy levels of a p-i-n diode are shown in Fig. 2a. In forward direction, electrons are injected from the n-doped and holes from the p-doped layer, and recombine in the intrinsic layer. In the reverse direction, the current is blocked at first. However, if the electric field inside the intrinsic layer becomes sufficiently large, electrons can tunnel from occupied HOMO (highest occupied molecular orbital) states to empty LUMO (lowest unoccupied molecular orbital) states, effectively generating free charge carriers.[21]

The current vs. voltage characteristic of the Zener-diode used here is shown in Fig. 2b. The device consists of an aluminum film (50 nm) as anode, 40 nm of p-doped Pentacene (F6-TCNNQ, 4 $wt.\%$), a thin layer of intrinsic Pentacene (55 - 105 nm), n-doped C_{60} (o-MeO-DMBI-I, 8 $wt.\%$, 40 nm), followed by another film of aluminum used as cathode (40

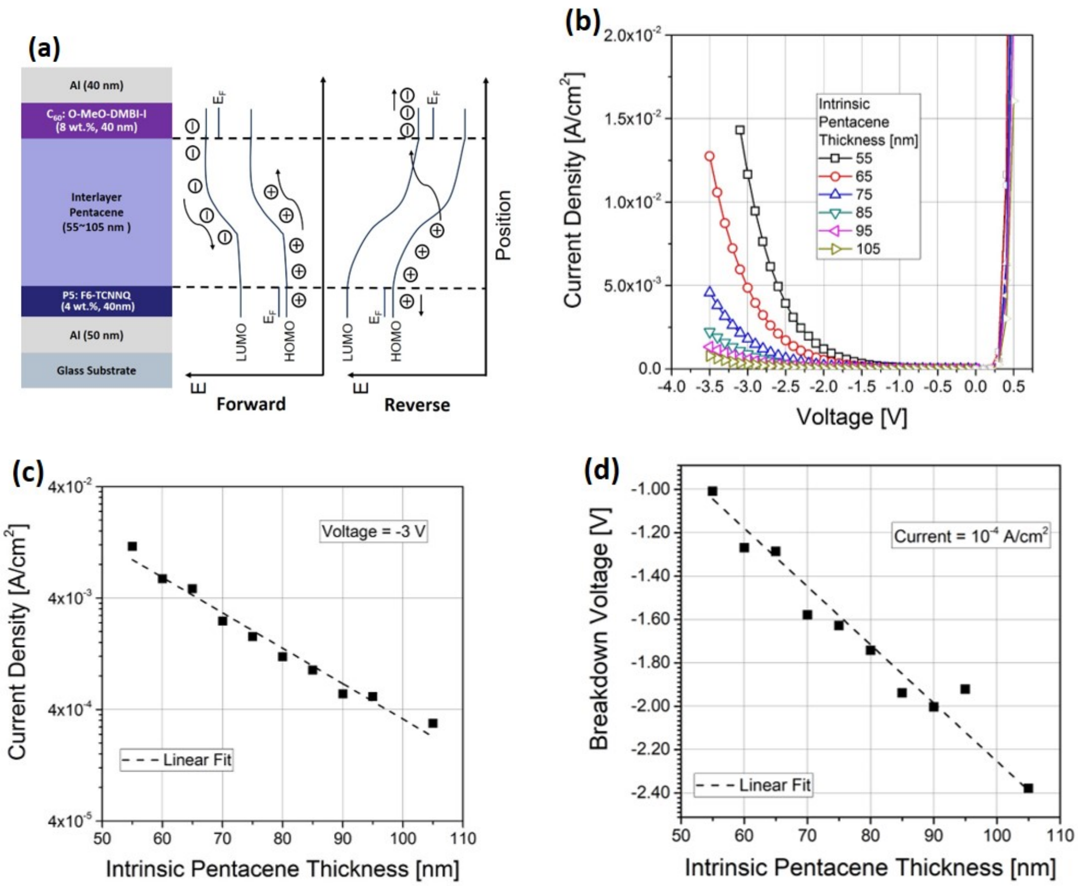

Figure 2: Characteristic of Pentacene/C_{60} based p-i-n Zener diodes. (a) Schematic device structure and energy level diagram. (b) Backward and forward current of the p-i-n Zener diodes for increasing thickness of the intrinsic Pentacene layer (from 55 to 105 nm). (c) The current density (measured at $V = -3\,V$) decreases exponentially with increasing thickness of intrinsic Pentacene. (d) The breakdown voltage (defined as voltage needed to reach a current density of 0.1 mA/cm^2) decreases linearly with increasing thickness of intrinsic Pentacene.

nm) (cf. Fig. 2a).

The device shows the expected behavior, indicative of Zener-tunneling:[21] in forward direction, the current increases exponentially with the voltage, but is almost independent of the thickness of the intrinsic interlayer (Fig. 2b). In backward direction, however, the current decreases exponentially with the intrinsic interlayer thickness (Fig. 2c). Furthermore, the breakdown voltage, defined as the voltage needed to reach a current density of 0.1 mA/cm^2, increases linearly with the intrinsic interlayer thickness (see Fig. 2d).

2.2 Organic Tunnel Field Effect Transistor - Device Concept

In order to turn the organic Zener diode shown in Fig. 2 into a VOTFET, a gate electrode has to be added to control the breakdown in the backward regime. Here, the setup shown in Fig. 3 is used. The top electrode is n-doped, whereas the electrodes in the middle are p-doped. Combined with the intrinsic Pentacene layer between the top and middle electrode, a p-i-n Zener-junction is formed, which is gated by the gate electrode on the bottom of the device.

The vertical OFETs can be operated in two distinct modes, depending on the polarity of the bias applied across the p-i-n Zener-junction: forward mode (the Zener junction is biased in forward direction) and backward or tunneling mode (the Zener junction is biased in backward direction). In both operation modes, a p-type channel is formed on top of the gate oxide if a negative potential is applied to the gate with respect to the source.

The forward mode is sketched in Fig. 3a. The top and middle electrodes serve as the drain and the source, respectively. Hence, a negative $V_{DS} < 0$ V is applied at the n-doped top electrode, whereas the p-doped middle electrode is kept at ground potential (GND). Fig. 3b shows the corresponding level diagram. Decreasing the gate-source voltage V_{GS} to more negative values moves the transport level in the channel up, which reduces the hole injection barrier at the source-channel interface, and thus, switches the device on. Holes are injected from the p-doped source electrode, transported through the channel of accumulated holes, and finally recombine with electrons injected at the drain.

Fig. 3c and 3d show the proposed working mechanism of the vertical transistor in the tunneling/backward mode. Here, a negative voltage is applied at the p-doped middle electrode that serves as drain ($V_{DS} < 0\ V$), while the top n-doped electrode held at ground potential serves as source. In the off-state (dashed line in Fig. 3d), a high injection barrier at the source blocks injection of charge carriers. However, decreasing the gate-source voltage V_{GS} to more negative values leads to an upward shift of the energy levels in the channel. Once the gate-source voltage is large enough to align the LUMO level of the source with the HOMO level of the channel, electrons can tunnel from the HOMO of the channel to the LUMO of the source by the same Zener-tunneling mechanism observed in Fig. 2. Effectively, free holes are generated in the channel, leaving behind free electrons at the source. Whereas the electrons in the source are extracted at the top contact, the holes in the channel accumulate at the oxide/semiconductor interface. Hence, the transistor turns from the off-state into the on-state.

In addition to the vertical structure sketched in Fig. 3a and 3c, neighboring middle electrodes form, together with the bottom gate, a conventional (unipolar) p-type OFET as well. Therefore, as shown in Fig. 4, the VOTFETs studied here have actually 4 terminals - two middle electrodes (p-doped), one top electrode (n-doped) and finally the gate electrode on the bottom.

To test the lateral OFETs, the two middle electrodes are used as drain and source, while the top electrode is left floating. When vertical OFETs are under test, the two middle electrodes share the same potential.

2.3 Forward Operation of Vertical OFETs

Fig. 5a shows the transfer characteristics of vertical OFETs (left) and corresponding lateral OFETs (right). The thickness of the intrinsic Pentacene between the middle and top electrode is kept constant at 65 nm. Three different transistors are shown in Fig. 5a, which

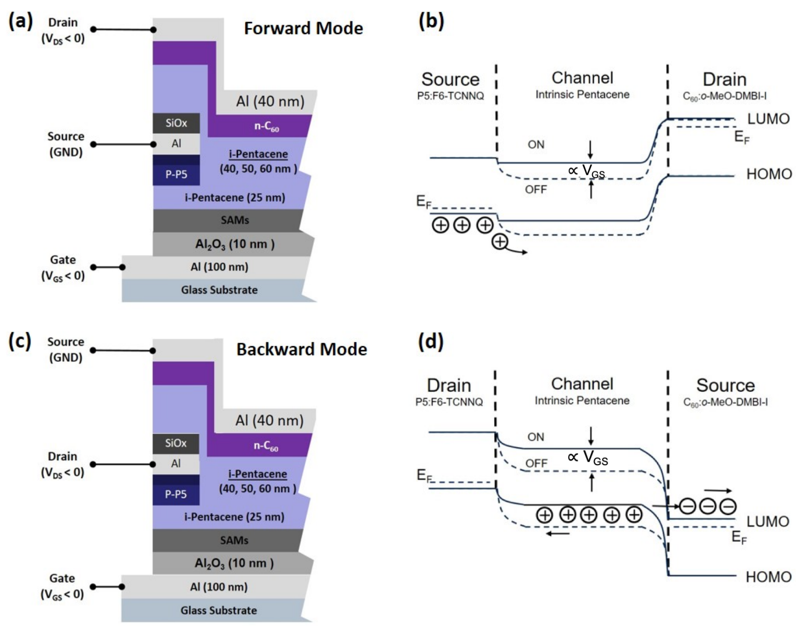

Figure 3: Device sketch and energy level diagram of the VOTFET operated in the forward or backward (tunneling) modes. In the diagram, dashed (solid) lines represent the off-state (on-state) of the transistor. (a) In forward operation, a negative drain-source voltage $V_{DS} < 0$ is applied to the top n-doped electrode and the middle p-doped electrode is kept at ground potential. (b) For $V_{GS} < 0$, an energy level upward shift inside the channel reduces the injection barrier at the source, which switches the device to the on-state. (c) In the tunneling mode, the drain-source voltage $V_{DS} < 0$ is applied to the middle p-doped electrode and the top n-doped electrode is kept at ground potential. (d) Upon reducing the gate-source voltage to more negative values ($V_{GS} < 0$), the HOMO level of the channel moves upwards, and once aligned with the LUMO level of the source, electrons can tunnel from the HOMO into the LUMO and the VOTFET switches on. Please note that the energy diagram sketched in (b) and (d) are approximations of the real energy landscape obtained under the assumption that the potential drops across the p-i and i-n contacts at the source and drain electrode only. In a real device, some of the applied potential will drop along the channel as well, leading to a slope of the energy levels in the HOMO/LUMO levels.

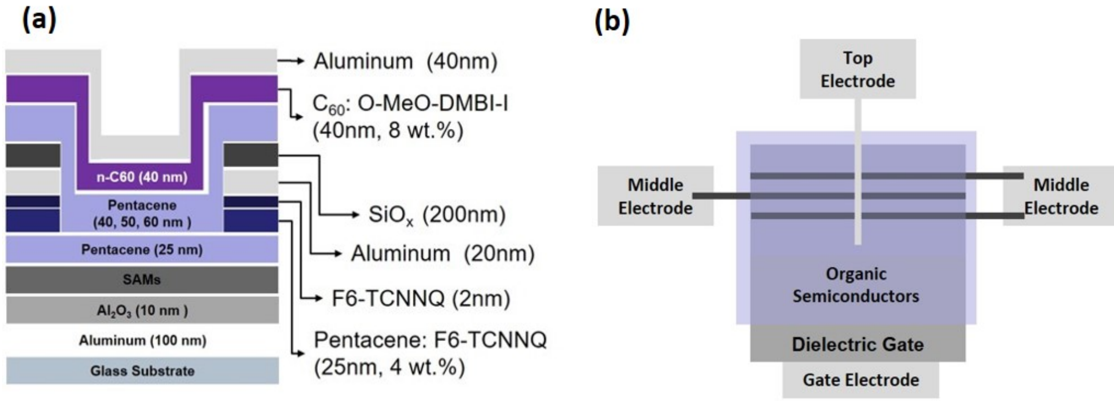

Figure 4: Cross-section (a) and top view (b) of the discussed VOTFETs. The organic injection layer at top electrode is n-doped. The injection layers at the two middle electrodes are p-doped, enabling regular lateral p-type operation.

differ by the distance between the two middle electrodes (i.e. the horizontal channel length). The two middle electrodes are used jointly as source electrodes when the vertical OFETs is measured. A drain voltage V_{DS} of -1.5 V is applied to the top n-doped electrode.

Both lateral and vertical OFETs have an ON/OFF ratio of about 10^4 and a charge mobility of 0.15 cm^2/Vs can be estimated from the transfer characteristics of the lateral OFETs on the bottom of the structure. The gate currents plotted in blue are below 10 nA.

From the proposed working mechanism of the vertical OFETs, it is expected that the on-current of VOFETs does not scale with the distance between neighboring middle electrodes, which is indeed observed in Fig. 5a (left). In the vertical geometry, all devices share the same intrinsic Pentacene layer thickness of 65 nm, which can be considered an effective channel length. The behavior changes if the lateral transistors are measured, i.e. if neighboring middle electrodes are used as source and drain electrodes and the top electrode is left floating. As expected, the drain current decreases inversely proportional to the channel length (see Fig. 5a, right panel).

Most importantly, the on-currents of vertical OFETs are higher than the ones of the lateral OFETs. In Fig. 5b, the transconductance of the lateral OFETs with 150 μm channel length and the corresponding vertical OFETs are plotted. The transconductance increases

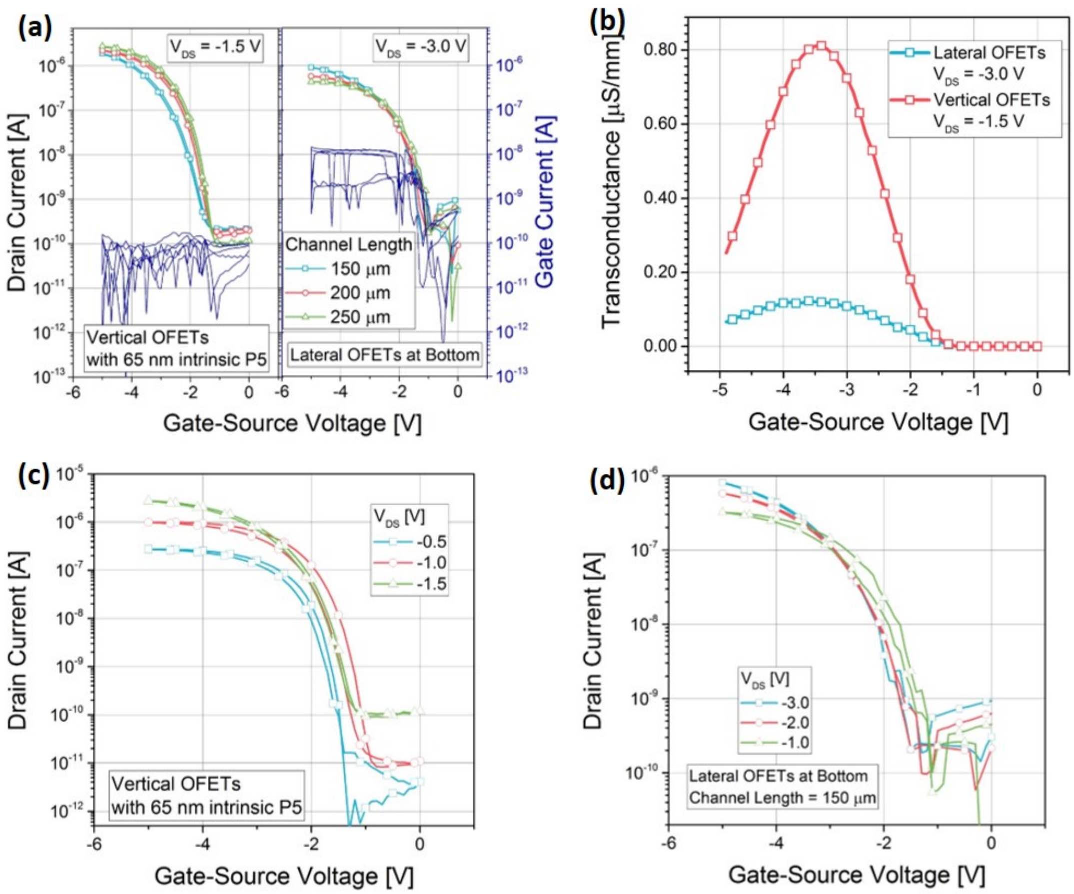

Figure 5: Electrical characteristics of vertical OFETs operated in the forward mode: (a) Transfer characteristics of the vertical (left panel) and corresponding lateral OFETs (right panel). (b) Comparison of the transconductance of the vertical and corresponding lateral OFET. The maximum transconductance per unit length for the vertical OFET (0.8 μS/mm) is almost 8 times higher than that of the lateral device (0.13 μS/mm). (c) Transfer characteristics of vertical OFETs measured in the forward mode for varying drain voltage. Both, the off- and on-current increase with V_{DS}. At V_{DS} = -0.5 V , the sub-threshold swing is about 122 mV/dec. (d) Transfer characteristics of lateral OFETs at different drain bias. The off-current remains in the 0.1 nA range and does not significantly increase with the drain voltage.

from 0.13 to 0.81 μS by switching from the lateral to the vertical configuration. Furthermore, the subthreshold swing decreases by more than a factor of two from 813.1 mV/dec to 340.2 mV/dec. This improvement in performance of the transistors is a result of scaling down the effective channel length in the vertical OFETs geometry.[4]

Fig. 5c and 5d plot the transfer characteristics of vertical and lateral OFETs at different drain voltages, respectively. Here, a striking difference between the vertical and horizontal OFETs is seen: For the vertical transistors, the off-current depends strongly on the drain potential, whereas for the lateral transistors no such dependency is observed. The increase in the off-current of vertical OFETs can be explained by considering that the off-current is due to forward currents of the p-i-n junction formed between source and drain (cf. Fig. 1b). In fact, the off-current at varying V_{DS} at $V_{GS} = 0\ V$ reflects the forward current of this p-i-n junction. Thus, the off-current of the vertical OFETs increases rapidly with increasing forward bias applied to the p-i-n junction, i.e. at increasing forward bias at the drain. However, if the drain potential is kept small (e.g. at V_{DS} = - 0.5 V), the drain potential is not sufficient to drive the p-i-n junction, which keeps the off-current low. Consequently, the device can be turned on quickly and the sub-threshold swing is further reduced to 122 mV/dec.

2.4 Tunnel Operation of Vertical OFETs

Fig. 6a shows the transfer characteristics of vertical OFETs operated in the tunneling mode measured at different drain voltages. The devices show a good transistor operation with an on/off switching ratio of approximately two orders of magnitude and a subthreshold swing of 970 mV/dec.

Fig. 6a further shows that the off-current and the on-current of the transistor increase with the drain voltage. The reason for the increase in off-current is similar to the forward case. The drain voltage presents a backward bias for the p-i-n junction formed between the source and drain of the vertical OFETs, and hence, the off-currents are determined by the

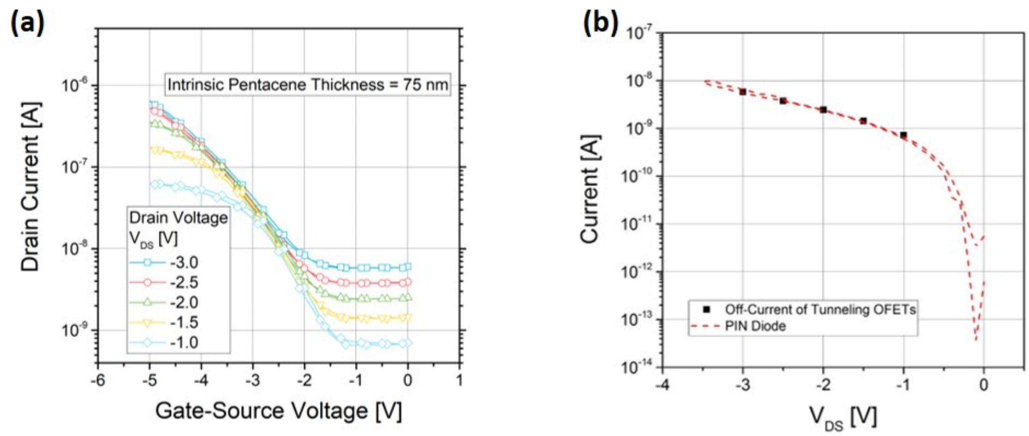

Figure 6: Electrical characteristics of the VOTFETs operated in the backward (tunneling) mode: (a) Transfer characteristics for different drain voltage. Both, the off-current and the on-current increase with decreasing V_{DS}. (b) Comparison of the reverse current of the p-i-n junction formed between source and drain (dashed line) and the off-current of the VOTFET in the backward mode at $V_{GS} = [-1.5\,\mathrm{V}, 0]$ (solid symbols).

reverse current of this backward operated p-i-n junction.

To validate this explanation, the backward current of the p-i-n junction measured between the top and middle electrodes (dashed line) is compared to the off-current extracted from the transfer curves in the voltage range of 0 V to -1.5 V (black symbols) in Fig. 6b. Indeed, a good agreement is found, adding confidence to the interpretation that the off-current of the vertical tunnel transistors is given by the backward current of the p-i-n junction between source and drain.

It was shown in previous reports on tunneling in reversely biased organic p-i-n diodes that the breakdown voltage can be adjusted by the intrinsic interlayer thickness of the p-i-n diode (cf. Fig. 2 as well).[21–23] The strong (exponential) dependency of the breakdown voltage on the interlayer thickness should hence provide a means to control the boundary between the on- and off-state of tunneling transistors, i.e. the threshold voltage. By tuning the intrinsic layer thickness, the breakdown voltage of the p-i-n junction between source and drain should change, i.e., the threshold voltage should increase for thicker intrinsic layers beyond the flatband voltage of the underlying MOS capacitance between source and gate electrode.

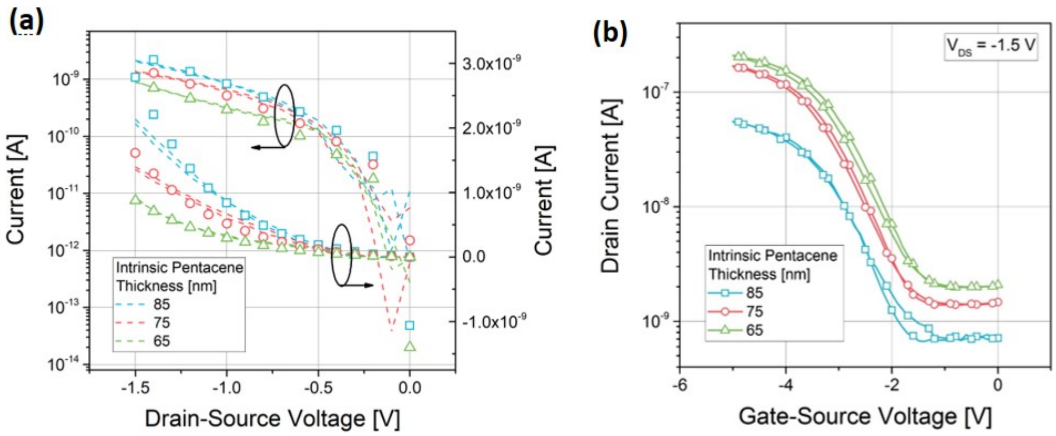

Figure 7: Impact of the intrinsic Pentacene thickness on VOTFETs in the backward mode: (a) Comparison of the backward currents of the p-i-n junction ($V_{GS} = 0\ V$) in the VOTFETs (dashed lines) and regular p-i-n diodes with the same thickness of intrinsic Pentacene (symbols). The agreement between the two measurements reiterates that a p-i-n junction is formed between the top and middle electrode. (b) Transfer characteristics of VOTFETs in backward mode: The on-set voltage shifts towards more negative V_{GS} for increasing thickness of the intrinsic Pentacene layer.

To test this hypothesis, the intrinsic layer thickness of the vertical transistor is varied from 65, 75 to 85 nm. The I-V characteristics of the p-i-n junction, measured between the source and drain keeping the gate potential at 0 V, for the different thicknesses of the intrinsic Pentacene layer, are plotted as dashed lines in Fig. 7a. Clearly, the backward current decreases with increasing thickness of the intrinsic Pentacene. To compare the p-i-n junction in the vertical transistor with the backward current of regular p-i-n diodes, the reverse current of the p-i-n diodes shown already in Fig. 2 is plotted as symbols in Fig. 7a as well. To match the current of the regular p-i-n diode with the current of the p-i-n junction in the vertical transistor, the area of the regular p-i-n diode is scaled down from 2.5×10^{-3} cm^2 (the original area of the processed p-i-n diodes) to 2.2×10^{-5} cm^2, indicating that the effective transistor area is much smaller than the area of regular p-i-n diodes. From this smaller effective area, the transfer length L_T of the vertical transistor (cf. Fig. 1b), i.e. the length holes are transported horizontally inside the transistor channel before being drained at the middle contact, can be estimated to approx. only $L_T = 1.36\ \mu m$. Reducing the distance between the middle electrodes below this transfer length might result in a reduced on-current of the transistors and might limit the scaling of this transistor type.

Fig. 7b plots the transfer characteristics of the vertical OFETs with different thickness of intrinsic Pentacene operated in the tunneling mode. As expected, the on-set voltage is shifted towards negative V_{GS} with increasing intrinsic Pentacene thickness. Overall, the threshold or on-set voltage decreases from -1.71 V to -1.95 V while the thickness of intrinsic Pentacene is increased from 65 to 85 nm. This finding demonstrates that the tunneling on-set is indeed delayed by increasing the thickness of intrinsic Pentacene, which is also observed in the corresponding p-i-n diode devices (cf. Fig. 2b).

The VOFET design is versatile and complementary n-type VOFETs can be realized by inversing the sequence of organic layers. As shown in Fig. 8a, the p-doped Pentacene layer is deposited on top and an n-doped C_{60} layer is used to improve injection at the middle electrode to yield an n-type tunnel transistor. Furthermore, in this second iteration of tunnel field-effect transistors, the intrinsic layer of Pentacene is replaced by C_{60}, which is known to form smoother films. In addition, the thickness of the gate oxide is reduced to 5 nm to reduce the operation voltage and optimize the subthreshold swing.

As shown in Fig. 8b, the transistors indeed operate at a significantly reduced voltage for both, the forward and backward mode, which can be explained by the thinner gate oxide. The subthreshold swing becomes 170.8 mV/dec and 190.3 mV/dec in the forward and backward operation mode, respectively. Besides, the same trends, in particular the same dependency on the drain potential, as for previous p-type transistors are observed.

2.5 Improved Saturation in Tunnel Transistors

As discussed in the introduction, the tunnel transistor presented here might provide an alternative approach to improve saturation of vertical OFETs. Due to the Zener junction included between source and drain (cf. Fig. 1b), the source should be shielded from the drain potential. In fact, direct leakage currents of holes from source to drain should be blocked by the n-doped film underneath the top electrode (for the p-VOTFET, Fig. 4a; p-doped for the

(a) (b)

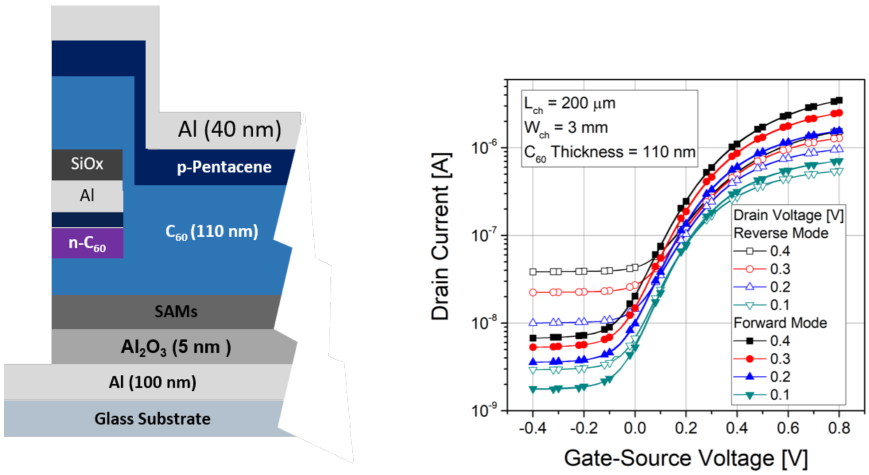

Figure 8: N-type VOTFETs can be realized by reversing the order of layers and replacing the intrinsic material by a thin layer of C_{60}(a). Due to the thinner gate dielectric, the operation voltage of the n-type transistor is reduced to below 1 V (b).

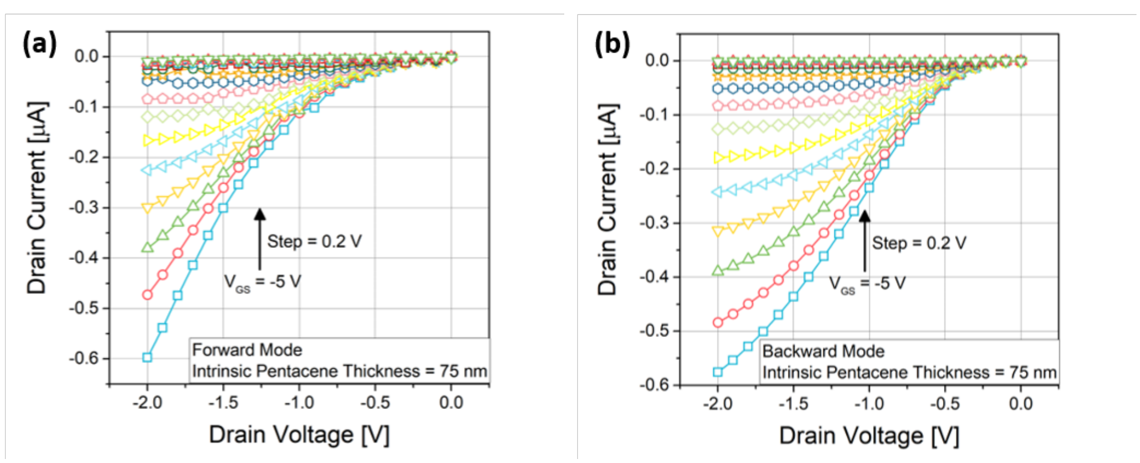

Figure 9: Output characteristic of the p-type VOTFET based on intrinsic Pentacene (see Fig. 4) operated in the forward (a) or backward (b) mode.

(a) (b)

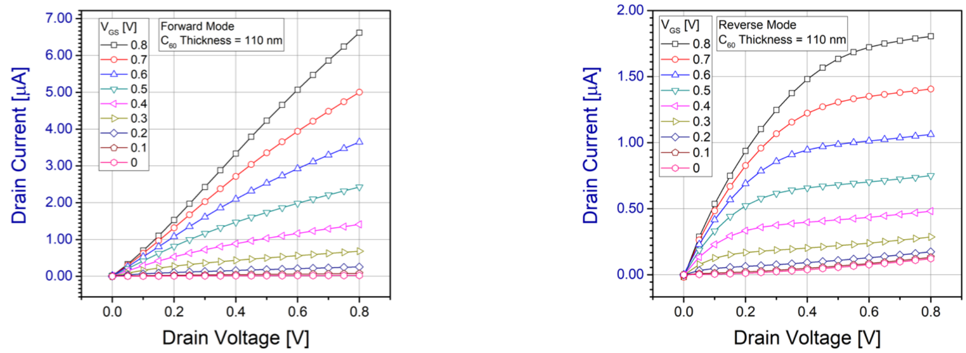

Figure 10: Output characteristic of the VOTFET based on intrinsic C_{60} (see Fig. 8a) operated in the forward (a) or backward (b) mode.

n-VOTFET, Fig. 8a), even if a direct contact of the drain electrode to the intrinsic layer is present at the edge of the source electrode.

Indeed, operating the transistors in the tunneling mode leads to an improved saturation in the output characteristics, which is shown in Fig. 9 for the devices based on intrinsic Pentacene and in Fig. 10 for the devices based on intrinsic C_{60}. The output characteristics of both, forward (Figs. 9a and 10a) and backward mode (Figs. 9b and 10b) are plotted. Most importantly, in the forward mode, the drain current continuously increases with the drain voltage without saturation as discussed in literature.[11] However, in contrast to the forward direction, the drain current reaches a saturation in the backward mode as observed in conventional OFETs.[27]

Comparing p-type and n-type transistors in Fig. 9 and Fig. 10, one observes that C_{60} based n-type transistors show less suppression of drain currents at low drain-source voltages, which is an indication for a lower contact resistance. The origin of the lower contact resistance is currently unknown. One possible reason for the improved injection is the higher gate capacitance of the n-type transistors, which will lead to a higher electric field at the contacts and hence a better injection.

2.6 Enhancing the Sub-threshold Swing of Organic Tunnel Transistors

Although the vertical transistors operated in the tunneling regime show a good performance, the subthreshold swings of 970 mV/dec observed in Fig. 6 and 190.3 mV/dec observed for the devices with thinner oxide layers and smoother intrinsic C_{60} layers are far from the benchmark value of 63 mV/dec, which sets the limit for conventional FETs. These rather large subthreshold swings are most likely caused by the performance of the underlying Zener diode shown in Fig. 2. In contrast to inorganic tunnel junctions,[19] the organic devices discussed here show a gradual increase in current rather than a sharp onset of the breakdown. This gradual increase in tunnel current widens the onset of the tunnel transistor, i.e. the increase in current in the subthreshold region is reduced.

To study the origin of this gradual onset of the tunnel current in organic Zener diodes and to be able to propose ways to improve device performance, an analytic I-V model of Zener diodes is presented in the supporting information. In the model, the tunnel current is calculated by

$$j = q\Gamma_0 \int_0^{d_i} \int_x^{d_i} \int_{-\infty}^{\infty} T(x,x') D_p(E,x) D_n(E,x') \left\{ f(E-E_{Fp}) - f(E-E_{Fn}) \right\} dE dx' dx \quad (1)$$

where Γ_0 is a constant tunnel rate, $T(x,x')$ is the tunnel probability from position x to x', $f(E)$ is the Fermi-Dirac distribution, and d_i is the thickness of the intrinsic layer. $D_p(E)$ and $D_n(E)$ are the density of states of holes and electrons, respectively, inside the intrinsic layer, and E_{Fn}, E_{Fp} are the quasi-Fermi levels of electrons and holes. Assuming Gaussian density of states for electrons and holes inside the intrinsic layers (with widths of σ_n and σ_p, respectively), and assuming a simple exponential decay of the tunnel probability $T(x,x') = T_0 \exp(-\gamma(x'-x))$ (γ: decay constant) one arrives at the following current-voltage characteristic

$$j(V) = -\int_0^{d_i} KT(\lambda) \left(\text{erf}\left(\frac{eV - E_0}{\sqrt{2}\sigma} \right) + \text{erf}\left(\frac{E_0}{\sqrt{2}\sigma} \right) \right) d\lambda, \tag{2}$$

where K and σ are defined by Equation 18 and 13 of the supporting information, respectively, $\lambda = x' - x$ is the tunnel distance, and $\text{erf}(x)$ is the error function.

The intrinsic Pentacene layer used in the Zener diode shown in Fig. 2 is known to be rough.[28] In order to include the effect of film roughness on the tunnel current, a probability function $P(t, d_i)$ is defined, which represents the probability to find a spot in the intrinsic layer of nominal thickness d_i with an actual thickness t. A Gaussian distribution with a standard deviation of σ_d is used for $P(t, d_i)$:

$$P(t, d_i) = \frac{1}{\sqrt{2\pi}\sigma_d} \exp\left(-\frac{(t - d_i)^2}{2\sigma_d^2} \right). \tag{3}$$

With the help of $P(t, d_i)$, the effective tunnel current inside the junction can be expressed as a sum over all $j(t)$ weighted by the probability $P(t)$

$$j = \int_{-\infty}^{\infty} P(t) j(t) dt \tag{4}$$

In Fig. 11a, the current-voltage characteristics of a p-i-n diodes with different thickness d_i of the intrinsic layer operated in reverse are plotted. The parameters used to calculate the current are chosen to resemble the Pentacene based diode shown in Fig. 2a (HOMO position $E_{0p} = 5\ \ eV$, LUMO position $E_{0n} = 3\ \ eV$, built-in voltage $V_{bi} = 1.8\ \ V$).

Indeed, the qualitative trends resemble the experimental result of Fig. 2. The diodes show significant currents above a certain breakdown voltage and the breakdown voltage increases linearly with the thickness of the intrinsic layer.

In addition, the Zener breakdown is influenced by the roughness of the intrinsic film,[28] which is shown in Fig. 11b. Increasing σ_d, i.e. the standard deviation of the Gaussian

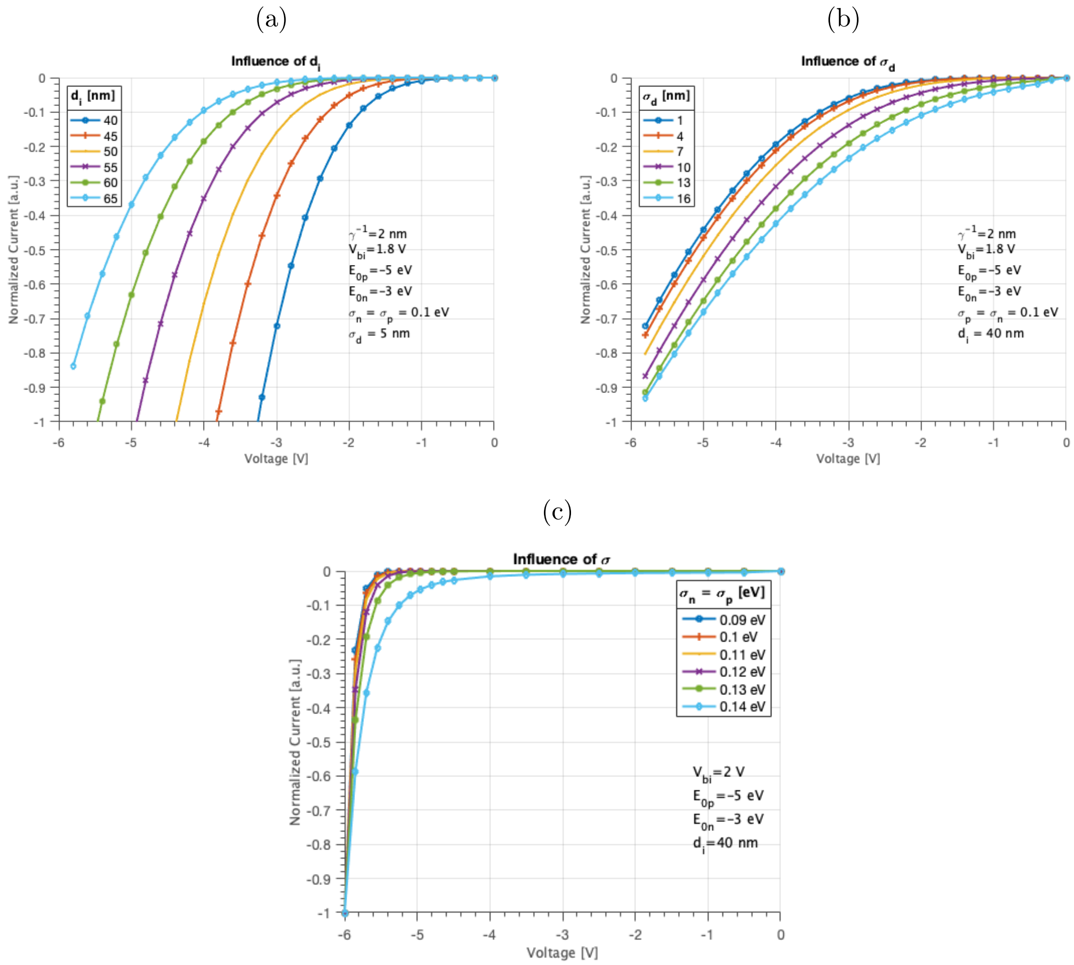

Figure 11: (a) and (b) Zener-Tunneling in organic p-i-n diodes as modeled by Equation 2. Details are described in the supporting information. The dependency of the tunnel current and Zener breakdown on the thickness d_i (a), and roughness σ_d of the intrinsic layer(b) is shown. In (c) the dependency of the tunnel current on the energetic width of the density of states (i.e. on σ_n and σ_p) is shown. The current was calculated taking an energy dependence of the tunnel probability into account (Equations 5 and 6).

distribution of thickness defined in Equation 3, leads to a shift of the I-V characteristic toward lower voltages. It appears that for an increased roughness, spots of smaller thickness start to dominate the overall characteristic of the diode, which leads to an increase in the tunnel current. Furthermore, the onset of the Zener breakdown is less sharp for rougher films and the current at low voltages increases. Again, this gradual onset in tunneling can be explained by an increasing contribution of tunnel currents in thinner parts of the device. Experimentally, this gradual onset of tunneling is observed in the characteristic of the two-terminal Zener diodes in Fig. 2, as well as in the Zener junction formed between the middle and top electrode of the VOTFET shown in Fig. 7.

Not only does the roughness of the intrinsic film weaken the steepness of the tunnel characteristic, but the energetic disorder in the intrinsic film (i.e. increased σ_n and σ_p) leads to a more gradual onset of the tunnel current as well. However, to correctly describe this effect, a more refined model for the tunnel coefficient $T(E,\lambda)$ has to be used. To derive Equation 2, it was assumed that the tunnel coefficient is independent on the tunnel energy, i.e. electrons tunnel at all energies with the same probability. By using this approximation, the tunnel coefficient $T(E,\lambda)$ could be taken out of the integral and the integration over the energy could be done analytically.

To correctly study the dependency of the tunnel current on the width of the gaussian distribution of states σ_n and σ_p, the energy dependence of the tunnel coefficient can be calculated by the WKB approximation

$$T(E,\lambda) \approx \exp\left(-\frac{2}{\hbar}\int_0^\lambda dx\sqrt{2m\left[E_{LUMO}(x)-E\right]}\right) \tag{5}$$

where $E_{LUMO} - E$ presents the effective tunnel barrier for an electron at energy E.

Using Equation 5, the energy integral of Equation 1 has to be solved numerically, leading to the following tunnel current ($f(E,x)$ is the Fermi-Dirac distribution)

$$j = q\Gamma_0 \int_0^{d_i} d_i \int_{-\infty}^{\infty} T(E,\lambda) D_p(E,x) D_n(E,x') \left[f(E - E_{Fp}, 0) - f(E - E_{Fn}, d_i) \right] dE d\lambda \quad (6)$$

The results of these calculations are shown in Fig. 11c, where the normalized current for increasing width of the density of states σ_n and σ_p is plotted vs. the applied voltage. The current is calculated for smooth films, i.e. the influence of roughness is neglected ($\sigma_d = 0$). Overall, the tunnel current strongly increases for larger σ, which can be explained by the increased overlap between the HOMO and LUMO density of states effectively reducing the tunnel barrier. However, not only does the absolute current increase, but the slope of the tunnel current decreases, i.e. on-switching of the diode becomes more gradual.

In summary, the energetic disorder in the intrinsic film and the roughness of the intrinsic layer limit the slope of the current rise in the breakdown regime. However, a sharp onset of the tunnel current is essential for a small subthreshold swing in tunnel transistors, i.e. the subthreshold swing of the tunnel OFETs discussed here is limited by the properties of the intrinsic organic layer. In order to decrease the subthreshold swing further, materials have to be found that present less disorder and form smoother films.

2.7 Conclusion

Vertical organic transistors are known to reach very high transconductance values, but often suffer from short channel effects, in particular a weak saturation in the output characteristic. Here, a new organic transistor design is proposed - the vertical organic tunnel field-effect transistor - that suppresses a direct source-drain leakage, and by that, improves the saturation performance.

Vertical OFETs operating in the forward and backward, i.e. tunneling mode are presented. Several trends are described that confirm the proposed tunneling mechanism in backward operated vertical OFETs: The off-current of the tunnel transistor is in good agreement with the backward current of the p-i-n junction formed between source and drain, which indicates that the current in the tunneling transistor indeed originates from the p-i-n junction. Furthermore, the output characteristics shows that the drain current saturates at large drain potentials and exhibits the same behavior as a p-i-n diode operated in reverse. Besides, the threshold voltage of the tunnel transistor can be tuned by the thickness of the intrinsic layer, which is interpreted as an increased breakdown voltage of the p-i-n junction.[21]

The tunnel transistors presented here open new ways to optimize the performance of vertical organic transistors. In particular, as shown here, the Zener junction included between source and drain electrode reduces direct currents flowing from source to drain and hence increases the saturation behavior of the transistors. Furthermore, the tunnel injection mode described here might provide a new approach to reduce injection losses, which are currently limiting OFET performance.[29]

Looking forward, there are clear ways to improve the performance of VOTFETs. As shown by a qualitative model of the underlying Zener diode, VOTFETs are currently limited by the electronic structure and morphology of the organic semiconductor. In order to decrease the subthreshold swing below 63 mV/dec and furthermore decrease the off-currents, materials have to be found that combine a high order (leading to a sharp density of states) with low film roughness (to suppress off-currents) in order to improve the performance of the VOTFETs further.

2.8 Experimental

Glass substrates are cleaned by sequential ultrasonication in D.I. water, Acetone, Methanol and Isopropanol. Nitrogen gas is used to dry the substrates.

An aluminum film of 100 nm is deposited by thermal evaporation onto the glass substrate and structured to form the gate via shadow masks. Afterwards, a thin aluminum oxide is grown by anodization[30] to form the gate dielectric. The thickness of the thin aluminum oxide is controlled by the terminating anodization voltage[30] and is about 10 nm to achieve low voltage operation of the transistors. The samples are immersed in 5 mM solution of N-tetradecylphosphonic acid (TDPA) overnight (18hr) to form a passivation layer of self-assembled monolayers (SAMs) on the oxide surface.[29] The samples are rinsed by Isopropanol and again dried by Nitrogen gas. Finally, samples are annealed for 20 min at 70 ^oC in a nitrogen filled glovebox. The ultra-high capacitance of such a thin Al_2O_3 gate covered by phosphoric acid based SAMs ensures that the lateral OFETs in the bottom structure and the vertical OFETs can be operated at voltages below 5 V, i.e. in the same voltage range of the vertical p-i-n diode.

Assembling the vertical transistors is split into two parts: fabrication of the bottom structure (cf. Fig. S5 of the supporting information) followed by preparation of the top part of the device (cf. Fig. 4).

The bottom structure itself forms a typical lateral OFET, in which a film of intrinsic Pentacene (25 nm) is used as the organic semiconductor layer. Both electrodes consist of 25 nm of heavily p-doped Pentacene (4 $wt.\%$ of Pentacene:F6-TCNNQ), followed by a thin film (2 nm) of pure F6-TCNNQ to ensure a good injection.[31] The contacts are formed by a thin aluminum film (20 nm). A film of silicon oxide (SiOx, 200 nm) is deposited on top of the electrodes by thermal evaporation to block unwanted currents that leak directly into the top structure. The bottom OFETs structures share the same channel width of 3 mm, while he channel length is varied from 150, 200 to 250 μm.

The top structure consists of a layer of intrinsic Pentacene (Fig. 4a, thickness of 40, 50 and 60 nm). Thus, including 25 nm of intrinsic Pentacene present in the bottom structure, the total thickness of intrinsic Pentacene is 65, 75 and 85 nm. This layer is followed by a 40 nm film of heavily n-doped C_{60} (8 $wt.\%$ of C_{60}: o-MeO-DMBI-I) and a thin aluminum electrode (40 nm) on top, which works as the n-type injection layer.

For C_{60}-based VOTFETs, the intrinsic layer is replaced by C_{60} (110nm), and its sequence of injection layer is inversed. The p-doped Pentacene layer (4 $wt.\%$ of Pentacene:F6-TCNNQ, 40 nm) is switched to the top electrode, and the n-doped C_{60} layer (8 $wt.\%$ of C_{60}:o-MeO-

DMBI-I, 25 *nm*) is used as the n-doped layer at the middle electrode, which is followed by a thin n-dopant film (o-MeO-DMBI-I, 2 *nm*) to enhance injection. Furthermore, the thickness of the gate oxide is reduced to 5 *nm* to reduce the operation voltage.

Regular p-i-n diodes are fabricated on cleaned glass substrates as well. Firstly, a film of aluminum (50 *nm*) is deposited as the bottom electrode. Then, a p-type injection layer (Pentacene:F6-TCNNQ, 4 *wt.*%, 40 *nm*), an interlayer (intrinsic Pentacene), and an n-type injection layer (C_{60}: o-MeO-DMBI-I, 8 *wt.*%, 40 *nm*) are sequencially deposited as shown in Fig. 2a. Finally, a film of aluminum (40 *nm*) is deposited as the top electrode. The overlapping area of the two aluminum electrodes defines the effective area of the p-i-n diode, which is a square with an area of $2.5 \times 10^{-3}\ cm^2$.

The devices are characterized using a Keithley SCS-4200 semiconductor parameter analyzer inside the glovebox at room temperature (300 K).

Aluminum and SiOx are purchased from Sigma-Aldrich with a purity of 99.999 % and 99.99 % respectively. The intrinsic material of Pentacene and C_{60} are purchased from Creaphys GmbH with a purity of 99.99 %. The n-dopant o-MeO-DMBI-I and the p-dopant F6-TCNNQ are purchased from Lumtech with a purity of 99.9 %. All materials are used without further purification.

Acknowledgement

The authors acknowledge funding from the National Science Foundation (EECS 1709479 and 1639073) and from the Binational Science Foundation (Grant No. 2014396). The research was further supported by competitive research funding from King Abdullah University of Science and Technology. Correspondence and requests for materials should be addressed to B.L. (email: blussem@kent.edu).

Supporting Information Available

A detailed description of the model used to describe Zener tunneling is provided in the supporting information.

References

(1) Rolin, C.; Kang, E.; Lee, J.-H.; Borghs, G.; Heremans, P.; Genoe, J. Charge carrier mobility in thin films of organic semiconductors by the gated van der Pauw method. *Nature Communications* **2017**, *8*, 14975.

(2) Klauk, H. Will We See Gigahertz Organic Transistors? *Advanced Electronic Materials* **2018**, *4*, 1700474.

(3) Lüssem, B.; Günther, A.; Fischer, A.; Kasemann, D.; Leo, K. Vertical organic transistors. *Journal of Physics: Condensed Matter* **2015**, *27*, 443003.

(4) Kleemann, H.; Günther, A. A.; Leo, K.; Lüssem, B. High-Performance Vertical Organic Transistors. *Small* **2013**, *9*, 3670–3677.

(5) Kwon, H.; Kim, M.; Cho, H.; Moon, H.; Lee, J.; Yoo, S. Toward High-Output Organic Vertical Field Effect Transistors: Key Design Parameters. *Advanced Functional Materials* **2016**, *26*, 6888–6895.

(6) Lee, G.; Lee, I.-H.; Park, H.-L.; Lee, S.-H.; Han, J.; Lee, C.; Keum, C.-M.; Lee, S.-D. Vertical organic light-emitting transistor showing a high current on/off ratio through dielectric encapsulation for the effective charge pathway. *Journal of Applied Physics* **2017**, *121*, 024502.

(7) Kim, C.-H.; Hlaing, H.; Kymissis, I. A macroscopic model for vertical graphene-organic semiconductor heterojunction field-effect transistors. *Organic Electronics* **2016**, *36*, 45–49.

(8) Hlaing, H.; Kim, C.-H.; Carta, F.; Nam, C.-Y.; Barton, R. A.; Petrone, N.; Hone, J.; Kymissis, I. Low-Voltage Organic Electronics Based on a Gate-Tunable Injection Barrier in Vertical graphene-organic Semiconductor Heterostructures. *Nano Letters* **2015**, *15*, 69–74.

(9) Swathi, K.; Narayan, K. S. Self-Assembled Porous Alumina Based Organic Nanotriode Arrays. *Nano Letters* **2017**, *17*, 7945–7950.

(10) Nakamura, K.; Hata, T.; Yoshizawa, A.; Obata, K.; Endo, H.; Kudo, K. Metal-insulator-semiconductor-type organic light-emitting transistor on plastic substrate. *Applied Physics Letters* **2006**, *89*, 103525.

(11) Greenman, M.; Sheleg, G.; Keum, C.-m.; Zucker, J.; Lüssem, B.; Tessler, N. Reaching saturation in patterned source vertical organic field effect transistors. *Journal of Applied Physics* **2017**, *121*, 204503.

(12) Yu, H.; Kim, D.; Lee, J.; Baek, S.; Lee, J.; Singh, R.; So, F. High-gain infrared-to-visible upconversion light-emitting phototransistor. *Nature Photonics* **2016**, *10*, 129.

(13) Hansch, W.; Fink, C.; Schulze, J.; Eisele, I. A vertical MOS-gated Esaki tunneling transistor in silicon. *Thin Solid Films* **2000**, *369*, 387–389.

(14) Aydin, C.; Zaslavsky, A.; Luryi, S.; Cristoloveanu, S.; Mariolle, D.; Fraboulet, D.; Deleonibus, S. Lateral interband tunneling transistor in silicon-on-insulator. *Applied Physics Letters* **2004**, *84*, 1780–1782.

(15) Wang, P.-F.; Hilsenbeck, K.; Nirschl, T.; Oswald, M.; Stepper, C.; Weis, M.; Schmitt-Landsiedel, D.; Hansch, W. Complementary tunneling transistor for low power application. *Solid-State Electronics* **2004**, *48*, 2281–2286.

(16) Bhuwalka, K. K.; Schulze, J.; Eisele, I. Performance enhancement of vertical tunnel

field-effect transistor with SiGe in the δp+ layer. *Japanese Journal of Applied Physics* **2004**, *43*, 4073.

(17) Appenzeller, J.; Lin, Y.-M.; Knoch, J.; Avouris, P. Band-to-band tunneling in carbon nanotube field-effect transistors. *Physical Review Letters* **2004**, *93*, 196805.

(18) Ionescu, A. M.; Riel, H. Tunnel field-effect transistors as energy-efficient electronic switches. *Nature* **2011**, *479*, 329.

(19) Shin, G. H.; Koo, B.; Park, H.; Woo, Y.; Lee, J. E.; Choi, S.-Y. Vertical-Tunnel Field-Effect Transistor Based on a SiliconâĂŞMoS2 Three-DimensionalâĂŞTwo-Dimensional Heterostructure. *ACS Applied Materials & Interfaces* **2018**, *10*, 40212–40218.

(20) Lu, Y.; Bangsaruntip, S.; Wang, X.; Zhang, L.; Nishi, Y.; Dai, H. DNA functionalization of carbon nanotubes for ultrathin atomic layer deposition of high κ dielectrics for nanotube transistors with 60 mv/decade switching. *Journal of the American Chemical Society* **2006**, *128*, 3518–3519.

(21) Kleemann, H.; Gutierrez, R.; Lindner, F.; Avdoshenko, S.; Manrique, P. D.; Lüssem, B.; Cuniberti, G.; Leo, K. Organic Zener diodes: tunneling across the gap in organic semiconductor materials. *Nano Letters* **2010**, *10*, 4929–4934.

(22) Keum, C.-M.; Liu, S.; Al-Shadeedi, A.; Kaphle, V.; Bunge, S. D.; Lüssem, B. Charge trapping in doped organic Zener diodes. *Organic Electronics* **2016**, *39*, 77–84.

(23) Al-Shadeedi, A.; Liu, S.; Keum, C.-M.; Kasemann, D.; Hoßbach, C.; Bartha, J.; Bunge, S. D.; Lüssem, B. Minority currents in n-doped organic transistors. *ACS Applied Materials & Interfaces* **2016**, *8*, 32432–32439.

(24) Perumal, A.; Fröbel, M.; Gorantla, S.; Gemming, T.; Lüssem, B.; Eckert, J.; Leo, K. Novel approach for alternating current (AC)-driven organic light-emitting devices. *Advanced Functional Materials* **2012**, *22*, 210–217.

(25) Hamwi, S.; Meyer, J.; Kröger, M.; Winkler, T.; Witte, M.; Riedl, T.; Kahn, A.; Kowalsky, W. The role of transition metal oxides in charge-generation layers for stacked organic light-emitting diodes. *Advanced Functional Materials* **2010**, *20*, 1762–1766.

(26) Rosenow, T. C.; Furno, M.; Reineke, S.; Olthof, S.; Lüssem, B.; Leo, K. Highly efficient white organic light-emitting diodes based on fluorescent blue emitters. *Journal of Applied Physics* **2010**, *108*, 113113.

(27) Liu, S.; Al-Shadeedi, A.; Kaphle, V.; Keum, C.-M.; Lüssem, B. Patterning organic transistors by dry-etching: The double layer lithography. *Organic Electronics* **2017**, *45*, 124–130.

(28) Guenther, A. A.; Widmer, J.; Kasemann, D.; Leo, K. Hole mobility in thermally evaporated pentacene: Morphological and directional dependence. *Applied Physics Letters* **2015**, *106*, 233301.

(29) Klauk, H.; Zschieschang, U.; Pflaum, J.; Halik, M. Ultralow-power organic complementary circuits. *Nature* **2007**, *445*, 745.

(30) Majewski, L.; Schroeder, R.; Voigt, M.; Grell, M. High performance organic transistors on cheap, commercial substrates. *Journal of Physics D: Applied Physics* **2004**, *37*, 3367.

(31) Günther, A. A.; Sawatzki, M.; Formánek, P.; Kasemann, D.; Leo, K. Contact Doping for Vertical Organic Field-Effect Transistors. *Advanced Functional Materials* **2016**, *26*, 768–775.